Journal of New Materials for Electrochemical Systems 17, 067-070 (2014)

Short Communication

Enhanced Catalytic Activity for the Ethanol Oxidation Reaction (EOR) using Novel Pt-Fe_3O_4/MWCNT Bimetallic Electrocatalyst

P.C. Meléndez González[1], Sagrario M. Montemayor[1], D. Morales Acosta[2,3], Y. Verde-Gómez[4,†], B. Escobar[4] and F.J. Rodríguez Varela[2,3,*]

[1]Departamento de Materiales Cerámicos, Facultad de Ciencias Químicas, Universidad Autónoma de Coahuila,V. Carranza s/n, Saltillo, Coahuila, México, C.P. 25280.
[2]Grupo de Sustentabilidad de los Recursos Naturales y Energía, Cinvestav Unidad Saltillo, Av. Industria Metalúrgica 1062, Parque Industrial Ramos Arizpe. Ramos Arizpe, Coahuila, C.P. 25900, México.
[3]Programa de Nanociencias y Nanotecnología, Cinvestav Unidad Saltillo.
[4]Instituto Tecnológico de Cancún, Av. Kabah Km 3, Cancún, Quintana Roo, 77500, México, Quintana Roo, 77500, México

Received: December 15, 2013, Accepted: January 25, 2014, Available online: April 15, 2014

Abstract: *In this work, 20% Pt-Fe_3O_4/MWCNT (Pt:Fe_3O_4 weight ratio of 80:20) and 20% Pt/MWCNT nanoparticles were synthesized and characterized as anode electrocatalysts in H_2SO_4 media. First, the electrocatalyst were submitted to accelerated catalyst degradation test (ACDT) by performing 500 cycles between 0.6 and 1.2 V (vs. SHE). Then, their performance for the EOR was evaluated. The magnetite-containing nanoparticles demonstrated to be highly electrochemically stable, with negligible surface area losses (less than 7%) in the hydrogen adsorption/desorption region. Moreover, Pt-Fe_3O_4/MWCNT showed a significantly enhanced catalytic activity for the EOR when compared to Pt/MWCNT, with almost 46% increase in current density when using Fe_3O_4 as co-catalysts.*

Keywords: MWCNTs; magnetite as co-catalyst; Pt-Fe_3O_4 electrocatalysts; ethanol oxidation reaction; Direct Alcohol Fuel Cells

1. INTRODUCTION

Direct Alcohol Fuel Cells (DAFCs) are having a growing attention of research groups worldwide because of their energetic advantages over other power conversion devices. Pt is the most widely used catalyst for fuel cell applications [1]. However, due to the formation of reaction intermediates, such as CO, acetaldehyde and acetic acid, the efficient electrooxidation of ethanol in DAFCs requires the use of metallic alloys or composite nanocatalysts at which the bifunctional mechanism takes place. Under these conditions, the kinetic of the EOR is faster and occurs at lower potentials when compared to Pt-alone materials.

It has been demonstrated that nanosized Pt-Sn/C is one of the most active alloys for the EOR [2-3]. Also, some Pt-metal oxides have shown an enhanced performance for the EOR. For example, Pt-CeO_2/C can promote the oxidation of ethanol and other organic molecules at more anodic potentials related to Pt-alone anodes [4]. Also, it has been shown that the use of a Pt-Ni-TiO_2NT/C anode can oxidize ethanol at lower potentials than Pt/C and Pt-Ni/C due to the interaction of the alloy with the TiO_2 nanotubes [5].

Recently, some authors have reported the use of iron oxides as relatively cheap and active co-catalyst. Fe_3O_4 and Fe_2O_3 have been studied in composite materials along with noble metals, for the oxidation of organic molecules and the Oxygen Reduction Reaction (ORR) [6-9]. The results are promissory, indicating that iron oxides in combination with Pt can promote the activation of the DAFCs anode and cathode reactions at lower overpotentials than Pt-alone in acid media [6-9]. For example, the work by Sun et al. shows that dumbbell-like Pt-Fe_3O_4 nanoparticles have a high catalytic activity for the ORR [6]. Moreover, the electrochemical characterization of Fe_3O_4@Pt core-shell nanostructures has revealed that their catalytic activity for the EOR is higher than that of Pt-alone nanoparticles [8]. Along with magnetite, the use of Fe_2O_3 as co-catalyst with Pt has demonstrated to be advantageous for the

To whom correspondence should be addressed:
*Email: javier.varela@cinvestav.edu.mx, Phone: +52 (844) 438-9600 ext. 8526
†Email: ysmaelverde@yahoo.com

oxidation of methanol [10].

Meanwhile, the most commonly used supports for nanoparticles are carbon black and activated carbons, with Vulcan XC-72 being the most representative. These carbonous materials have been investigated in long term performance tests, and it has been found that they are prone to be oxidized in a fuel cell environment. Multi-Walled Carbon Nanotubes (MWCNTs) have been considered as an attractive fuel cell catalyst support due to their feasibility to deposit very well dispersed metal nanoparticles [11-13]. Also, because of their interesting properties such as nanometric size, highly accessible surface area, excellent corrosion resistance, good electrical conductivity, long term stability, and a positive interaction with the active phase [14, 15].

In this work, the synthesis of Pt-Fe_3O_4 supported on Multi-Walled Carbon Nanotubes (Pt-Fe_3O_4/MWCNT) is presented. The electrochemical stability of this anode is tested by ACDT, and its catalytic activity towards the EOR is evaluated and compared to that of a Pt/MWCNT anode. The materials characterization by XRD and HR-STEM is also discussed.

2. EXPERIMENTAL

2.1. Synthesis of MWCNTs

The MWCNTs used as support were synthesized by a modified chemical vapor deposition method (M-CVD) using Vycor tubing as substrate. Ferrocene ($Fe(C_5H_5)_2$, Aldrich) and toluene ($C_6H_5CH_3$, J. T. Baker) 0.255 mM solutions were pre-heated prior to injection into a tubular furnace. Argon gas was used to carry the precursor mixture into the Vycor tubing placed inside the furnace at 1173 K. The MWCNTs were treated with nitric acid in a reflux system in order to remove the remaining iron and amorphous carbon. Finally, the MWCNTs were washed several times with triple distilled water [11].

2.2. Synthesis of 20% Pt-Fe_3O_4/MWCNT

MWCNTs were dispersed in distilled water for 2 h using mechanical stirring with an Ultra-Turrax© T18 apparatus (UT), at 300 rpm. Then, the temperature of the reaction was set at 5 °C and kept in this value during the process. Separately, ethanol solutions of $H_2PtCl_66H_2O$ and $Fe(NO_3)_39H_2O$ (both from Aldrich) were prepared. In a typical synthesis, the required amount of $NaBH_4$ (Aldrich) needed to reduce the iron oxide precursor was added to the solution containing MWCNTs, followed by the addition of the ethanolic magnetite solution. The suspension was stirred by UT for 2h. Afterwards, the solution was adjusted by adding the amount of $NaBH_4$ needed to reduce the chloroplatinic acid, which was subsequently dispersed drop by drop into the mixture. The obtained solution was stirred again for 2h by UT. Then, the recovered powders were washed three times in distilled water by centrifugation at 5000 rpm for 10 min. The Pt:Fe_3O_4 weight ratio was 80:20.

Similarly, 20% Pt/MWCNT nanoparticles were obtained using the previous methodology, only eliminating the addition of the magnetite precursor.

2.3. Physicochemical characterization

The obtained catalysts were characterized by recording XRD in a Philips X-pert diffractometer using Cu Kα radiation operating at 40 kV using a Cu Ka radiation source ($\lambda_{K\alpha1}$=1.54060 Å). Diffractograms were acquired over 10-80 degrees with 0.025 steps. The

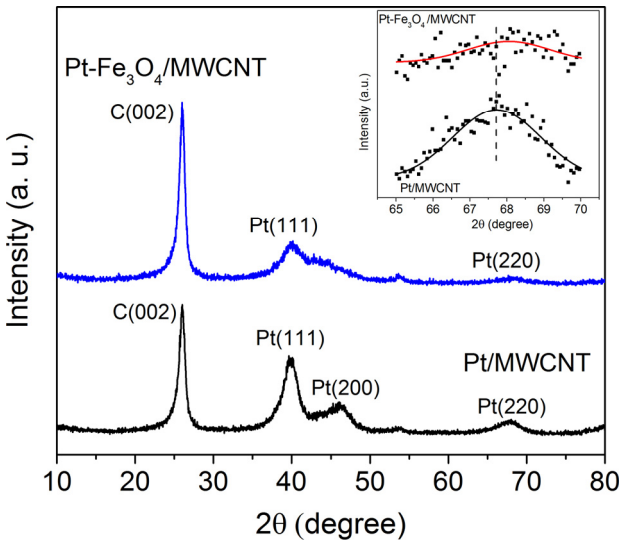

Figure 1. XRD patterns of Pt/MWCNT and Pt-Fe_3O_4/MWCNT. Insert shows the (220) peaks with experimental (scatter data) and fitting curves (solid lines).

XRD patterns were identified with the JCPDS data base. The chemical composition was evaluated by EDS in a Philips XL30 SEM apparatus using an accelerating voltage of 20 kV. Their morphology was analyzed by HAADF-STEM in a JEOL JEM-ARM200F microscope operating at 200 kV.

2.4. Electrochemical set-up and characterization

The catalytic inks were separately prepared by dispersing 10 mg of each nanocatalyst in a mixture of 1 ml propanol and 5 ml Nafion® solution, with a subsequent sonication for 30 min. Then, an aliquot of 10 ml of each material was deposited on a glassy carbon disc (5 mm diameter) embedded in a rotating disc set-up (Pine Inst.), which was used as working electrode after solvent evaporation. The counter electrode was a Pt mesh, while an Ag/AgCl was used as the reference electrode. However, in this work, all potentials were reported against the Standard Hydrogen Electrode (SHE).

Cyclic voltammograms (CVs) of the nanocatalysts were acquired in N_2-saturated 0.5 M H_2SO_4 at 20 mV s^{-1} between the potential interval of 0.05 V and 1.2 V, using a Voltalab PGZ301 potentiostat. ACDTs were done by performing potential cycling between 0.6 V and 1.2V at 75 mV s^{-1} for 500 cycles. After this test, CVs at 20 mV s^{-1} were carried out again. The electrochemical stability of the Pt-Fe_3O_4/MWCNT anode was established by evaluating the changes in the electrochemically active surface area (EASA), in the hydrogen adsorption/desorption region. Polarization curves of the EOR were acquired between 0.05 V and 1.2 V in a 0.5 M H_2SO_4 + 0.5M C_2H_5OH solution at 20 mV s^{-1}.

3. RESULTS AND DISCUSSION

Figure 1 shows the XRD patterns of Pt/MWCNT and Pt-Fe_3O_4/MWCNT. Characteristic (111), (200) and (220) peaks attributed to crystalline fcc platinum can be observed in both nanomaterials. Moreover, the (002) and (004) reflections of graphite 2H

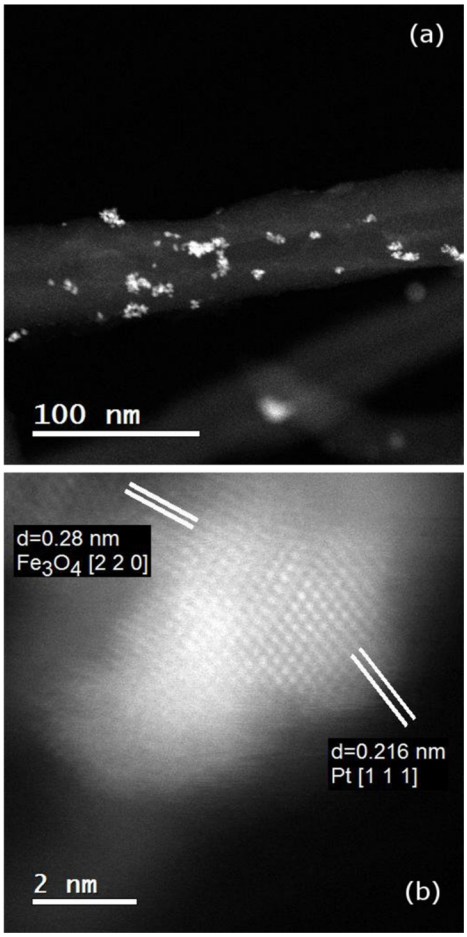

Figure 2. (a) STEM and (b) HR-STEM images from Pt-Fe_3O_4/MWCNT.

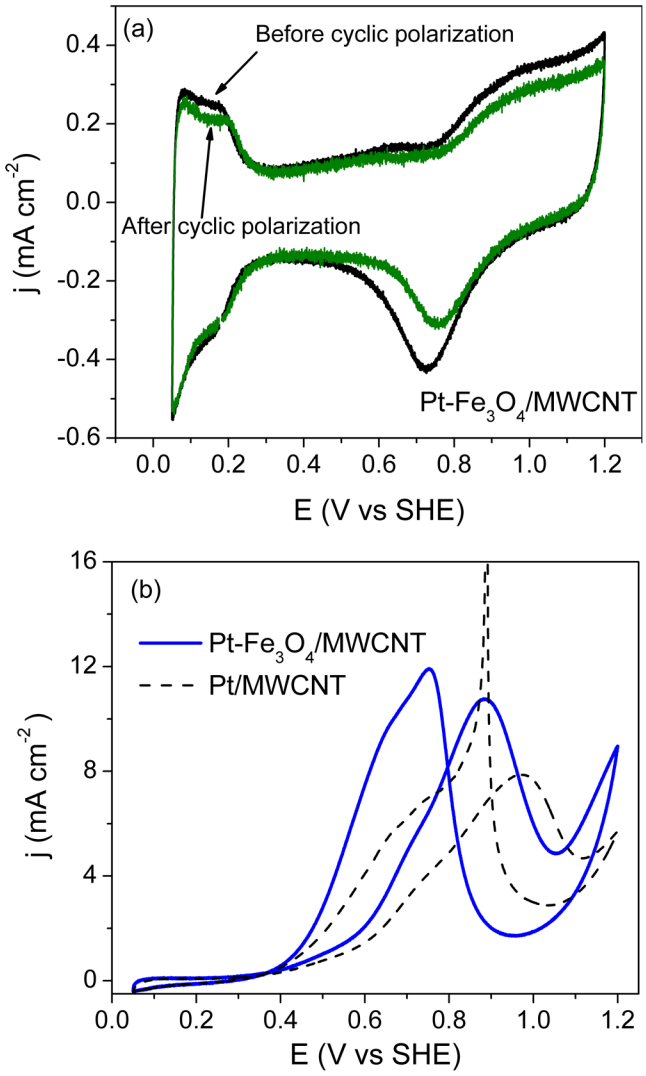

Figure 3. (a) CVs of Pt-Fe_3O_4/MWCNT before and after cyclic polarization in N_2-saturated 0.5 M H_2SO_4. (b) Polarization curves of the EOR at Pt-Fe_3O_4/MWCNT and Pt/MWCNT in N_2-saturated 0.5 M H_2SO_4 + 0.5 M C_2H_5OH electrolyte. Scan rate: 20 mV s^{-1}.

phase corresponding to the MWCNTs, also emerge at nearly 2q=26 and 54 degrees in both patterns. No diffraction peaks related to magnetite are identified in the case of the Pt-Fe_3O_4/MWCNT catalyst. Such characteristic differs from that of Fe_3O_4@Pt core-shell nanostructures reported elsewhere, at which magnetite reflections could be indexed [8-9]. This difference can be attributed to the magnetite content in the catalyst, which is higher at Fe_3O_4@Pt (see refs. [8-9]) compared to Pt-Fe_3O_4/MWCNT (this work).

A shift in the (220) diffraction peak of Pt-Fe_3O_4/MWCNT related to the corresponding peak of the Pt-alone catalyst can be observed in the insert of Figure 1. Thus, a lattice contraction is revealed by a lower value in the lattice parameter of Pt-Fe_3O_4/MWCNT (3.88 Å) compared to Pt/MWCNT (3.90 Å). This compression is attributed to an interaction between Fe_3O_4 and Pt atoms in the fcc structure. The values of particle size, calculated from the (220) diffraction peaks with the aid of the Scherrer equation, are 2.6 and 2.3 nm for Pt/MWCNT and Pt-Fe_3O_4/MWCNT, respectively (Table 1).

Figure 2 shows STEM images of Pt-Fe_3O_4/MWCNT. In Figure 2(a), Pt-Fe_3O_4 nanoparticles are distributed along the CNT forming some agglomerates. The HR-STEM image in Figure 2(b) shows details of Pt-Fe_3O_4 nanoparticles. From selected area electron diffraction (SAED) patterns and Fast Fourier Transform analysis, the interplanar distances were determined as *d*=0.216 and 0.28 nm,

Table 1. Chemical composition and average particle size of the electrocatalysts

Electrocatalyst	Pt (wt. %)	Fe_3O_4 (wt. %)	O (wt. %)	C (wt. %)	Pt:Fe_3O_4 wt. ratio	Particle size (nm)
Pt-Fe_3O_4/MWCNT	13.73	3.62	2.77	79.88	70:30	2.3
Pt/MWCNT	20.36	-	-	79.64	-	2.6

ascribed to Pt (111) and Fe_3O_4 (220) respectively. Figure 2(b) confirms the formation of the Pt-metal oxide catalyst.

The chemical composition of Pt-Fe_3O_4/MWCNT and Pt/MWCNT is shown in Table 1. For both electrocatalysts, the results confirm roughly 80 wt. % of Vulcan, in good agreement with the nominal calculations. The monometallic anode has a Pt content of 20.36 wt. %, i.e., the expected chemical composition. The chemical analysis of Pt-Fe_3O_4/MWCNT shows Pt, Fe_3O_4 and O contents of 13.73, 3.62 and 2.77 wt. %, respectively. The O detected for this material is considered to be due to the presence of the iron oxide. Thus, the Pt:Fe_3O_4 wt. ratio of Pt-Fe_3O_4/MWCNT is roughly 70:30, below the 80:20 nominal composition.

Figure 3(a) shows the CVs of the Pt-Fe_3O_4/MWCNT nanomaterial before and after ACDT. Even though there is a difference in the intensity of the PtO formation/reduction region after stability test, the changes in the hydrogen adsorption/desorption remain negligible. An evaluation of this region demonstrates the high electrochemical stability of the magnetite-containing anode. The surface area loss of this material after cyclic polarization is less than 7%. Meanwhile, the loss in the Pt/MWCNT anode (CVs not shown) is of about 5%, i.e., the stability of Pt-Fe_3O_4/MWCNT is as good as that of Pt-alone. The stability behavior of Pt-Fe_3O_4/MWCNT is similar to that of Fe_3O_4@Pt nanostructures reported elsewhere [8, 9]. However, it should be mentioned that in the material synthesized in this work there is no Pt shell covering a magnetite core as in references [8, 9], suggesting that the interaction of Pt with iron oxide in a bimetallic configuration also enhances the stability of the latter in H_2SO_4 electrolyte. More studies need to be carried out in order to fully understand the mechanism that promotes the high stability of Fe_3O_4 in acid electrolyte shown in Figure 3(a).

Figure 3(b) shows the polarization curves of the EOR at both electrocatalysts. Clearly, the catalytic activity of Pt-Fe_3O_4/MWCNT is higher than that of Pt/MWCNT. The onset potentials of the EOR are around 0.39 and 0.45 V (vs. SHE), while the maximum peak current densities in the positive scan are 11 and 7.5 mA cm^{-2} in Pt-Fe_3O_4/MWCNT and Pt/MWCNT, respectively. It means that almost 46% of increment in current density is due to the use of Fe_3O_4 as co-catalyst. Moreover, the peak maximum at Pt-Fe_3O_4/MWCNT is nearly 100 mV more negative compared to Pt-alone.

4. CONCLUSIONS

Pt-Fe_3O_4/MWCNT nanocatalysts were successfully synthesized by incipient wetness method and reduced with $NaBH_4$. Crystalline nanoparticles having a particle size of less than 3 nm were formed, according to XRD analysis. SAED and Fast Fourier Transform analysis of HR-STEM images allowed to identify lattice fringes attributed to Pt (111) and Fe_3O_4 (220) planes, confirming the formation of the Pt-Fe_3O_4/MWCNT nanoparticles. The chemical composition analysis of the bimetallic anode confirmed the presence of Pt, Fe_3O_4 and O. However, the Pt:Fe_3O_4 wt. ratio was 70:30, below the 80:20 nominal chemical composition.

The electrochemical characterization showed that Pt-Fe_3O_4/MWCNT is highly stable in acid media. The surface area loss of this anode after ACDT between 0.6 and 1.2 V (vs. SHE) was about 7% in 0.5M H_2SO_4 electrolyte. The polarization curves of the EOR demonstrated the higher catalytic activity of the magnetite-containing nanocatalyst compared to a Pt/MWCNT material. The Pt-Fe_3O_4/MWCNT anode outperformed Pt/MWCNT in terms of onset potential of the EOR, maximum current density peak in the positive scan and the position (potential) of the peak maximum. The results presented in this work indicate that a relatively cheap material such as magnetite could be used as co-catalysts along with Pt, and contribute in decreasing the costs of fuel cells electrocatalysts.

5. ACKNOWLEDGEMENTS

We thank CONACYT Mexico (Proyectos Bilaterales) for financing this project under grant No.164251. D.M.A. thanks the support of CONACYT under the Postdoctoral Fellowships Program. Authors also acknowledge the financial support of FOMIX CONACYT–Gob. de Quintana Roo, under grant No. QR00-2011-001-174895.

REFERENCES

[1] S.Q. Song, W.J. Zhou, Z.H. Zhou, L.H. Jiang, G.Q. Sun, Q. Xin, V. Leontidis, S. Kontou, P. Tsiakaras, Int. J. Hydrogen Energy, 30, 995 (2005).

[2] F.J. Rodríguez Varela, O. Savadogo, J. Electrochem. Soc., 155, B618 (2008).

[3] Sergio García-Rodríguez, Ferenc Somodi, Irina Borbáth, József L. Margitfalvi, Miguel Antonio Peña, Jose Luis G. Fierro, Sergio Rojas, Appl. Catal. B: Environ., 91, 83 (2009).

[4] R.F.B. De Souza, A.E.A. Flausino, D.C. Rascio, R.T.S. Oliveira, E. Teixeira Neto, M.L. Calegaro, M.C. Santos, Appl. Catal. B: Environ., 91, 516 (2009).

[5] Lei Shen, Qi-Zhong Jiang, Tao Gan, Min Shen, F.J. Rodriguez Varela, A.L. Ocampo, Zi-Feng Ma, J. New Mat. Electrochem. Systems, 13, 205 (2010).

[6] C. Wang, H. Daimon, S. Sun, Nano Lett., 9, 1493 (2009).

[7] L. Lai, G. Huang, X. Wang, J. Weng, Carbon, 49, 1581 (2011).

[8] N.M. Sánchez-Padilla, S.M. Montemayor, L.A. Torres, F.J. Rodríguez Varela, Int. J. Hydrogen Energy, 38, 12681 (2013).

[9] Nora Mayté Sánchez-Padilla, Sagrario M. Montemayor, F.J. Rodríguez Varela, J. New Mat. Electrochem. Systems, 15, 171 (2012).

[10] Yan-Ting Liu, Qin-Bo Yuan, Dong-Hong Duan, Zhong-Lin Zhang, Xiao-Gang Hao, Guo-Qiang Wei, Shi-Bin Liu, J. Power Sources, 243, 622 (2013).

[11] B. Escobar, R. Barbosa, M. Miki Yoshida, Y. Verde Gomez, J. Power Sources 243, 88 (2013).

[12] J. Li, Y. Liang, Q. Liao, X. Zhu, X. Tian, Electrochim. Acta, 54, 1277 (2009).

[13] Ana M. Valenzuela-Muñíz, Gabriel Alonso-Nuñez, Mario Miki-Yoshida, Gerardine G. Botte, Ysmael Verde-Gómez, Int. J. Hydrogen Energy, 38, 12640 (2013).

[14] A.L. Reddy, S. Ramaprabhu, J. Phys. Chem., C 111, 16138 (2007).

[15] Jiwei Ma, Aurélien Habrioux, Cláudia Morais, Adam Lewera, Walter Vogel, Ysmael Verde-Gómez, Guadalupe Ramos-Sanchez, Perla B. Balbuena, Nicolas Alonso-Vante, ACS Ca-